



The influence of water mass mixing on the dissolved Si isotope composition in the Eastern Equatorial Pacific



Patricia Grasse^{a,*}, Claudia Ehlert^{a,b}, Martin Frank^a

^a GEOMAR Helmholtz Centre for Ocean Research Kiel, Wischhofstrasse 1-3, 24148 Kiel, Germany

^b Max Planck Research Group for Marine Isotope Geochemistry, Institute for Chemistry and Biology of the Marine Environment (ICBM), University of Oldenburg, Carl-von-Ossietzky-Str. 9-11, 26129 Oldenburg, Germany

ARTICLE INFO

Article history:

Received 25 January 2013

Received in revised form 23 July 2013

Accepted 26 July 2013

Available online xxxx

Editor: G. Henderson

Keywords:

silicon isotopes

oxygen minimum zones

silicon cycle

upwelling area

SFB754

ABSTRACT

Silicon isotopes are a powerful tool to investigate the cycling of dissolved silicon (Si). In this study the distribution of the Si isotope composition of dissolved silicic acid ($\delta^{30}\text{Si}(\text{OH})_4$) was analyzed in the water column of the Eastern Equatorial Pacific (EEP) where one of the globally largest Oxygen Minimum Zones (OMZs) is located. Samples were collected at 7 stations along two meridional transects from the equator to 14°S at 85°50'W and 82°00'W off the Ecuadorian and Peruvian coast. Surface waters show a large range in isotope compositions $\delta^{30}\text{Si}(\text{OH})_4$ (+2.2‰ to +4.4‰) with the highest values found at the southernmost station at 14°S. This station also revealed the most depleted silicic acid concentrations (0.2 $\mu\text{mol/kg}$), which is a function of the high degree of Si utilization by diatoms and admixture with waters from highly productive areas. Samples within the upper water column and the OMZ at oxygen concentrations below 10 $\mu\text{mol/kg}$ are characterized by a large range in $\delta^{30}\text{Si}(\text{OH})_4$, which mainly reflects advection and mixing of different water masses, even though the highly dynamic hydrographic system of the upwelling area off Peru does not allow the identification of clear Si isotope signals for distinct water masses. Therefore we cannot rule out that also dissolution processes have an influence on the $\delta^{30}\text{Si}(\text{OH})_4$ signature in the subsurface water column. Deep water masses (> 2000 m) in the study area show a mean $\delta^{30}\text{Si}(\text{OH})_4$ of $+1.2 \pm 0.2\text{‰}$, which is in agreement with previous studies from the eastern and central Pacific. Comparison of the new deep water data of this study and previously published data from the central Pacific and Southern Ocean reveal substantially higher $\delta^{30}\text{Si}(\text{OH})_4$ values than deep water signatures from the North Pacific. As there is no clear correlation between $\delta^{30}\text{Si}(\text{OH})_4$ and silicic acid concentrations in the entire data set the distribution of $\delta^{30}\text{Si}(\text{OH})_4$ signatures in deep waters of the Pacific is considered to be mainly a consequence of the mixing of several end member water masses with distinct Si isotope signatures including Lower Circumpolar Deep Water (LCDW) and North Pacific Deep Water (NPDW).

© 2013 Elsevier B.V. All rights reserved.

1. Introduction

The silicon isotope composition of dissolved silicic acid ($\delta^{30}\text{Si}(\text{OH})_4$) is an important tool to investigate the biogeochemical cycling of silicon (Si). Besides nitrate (NO_3^-) and phosphate (PO_4^{3-}) silicic acid ($\text{Si}(\text{OH})_4$) is a major nutrient for diatoms, which require $\text{Si}(\text{OH})_4$ to build up their frustules (Lewin, 1961). The $\delta^{30}\text{Si}(\text{OH})_4$ signature not only helps to understand the biogeochemical cycling of Si in the modern ocean but via its incorporation into diatom frustules it is also an important proxy for the reconstruction of silicic acid utilization in the past (De la Rocha et al., 1998; Reynolds et al., 2008; Pichevin et al., 2009; Ehlert et al., 2013).

* Corresponding author. Tel.: +49 (0) 431 600 2259; fax: +49 (0) 431 600 2925.
E-mail address: pgrasse@geomar.de (P. Grasse).

The main factor controlling $\delta^{30}\text{Si}(\text{OH})_4$ in surface waters is $\text{Si}(\text{OH})_4$ utilization. Diatoms preferentially incorporate the lighter Si isotopes into their frustules thereby leaving seawater enriched in the heavy isotopes. Based on the few available data the enrichment factor (ε) between seawater and diatoms until recently appeared to be independent of species and temperature at a value near -1.1‰ (De la Rocha et al., 1997) whereas somewhat higher values of -1.5 to -1.8‰ were found by Milligan et al. (2004). New culture experiments on polar and subpolar diatom species show that ε can be species dependent encompassing a large range of -0.5 to -2.1‰ (Sutton et al., 2013). Apart from utilization, the dissolved $\delta^{30}\text{Si}(\text{OH})_4$ signal is influenced by mixing of water masses (Reynolds et al., 2006; Fripiat et al., 2011) and remineralization of the diatom opal in subsurface waters. Laboratory experiments by Demarest et al. (2009) indicate that isotopic fractionation with a factor of -0.55‰ occurs during partial dissolution of diatom biogenic silica (bSiO₂) thus preferentially releasing the lighter Si

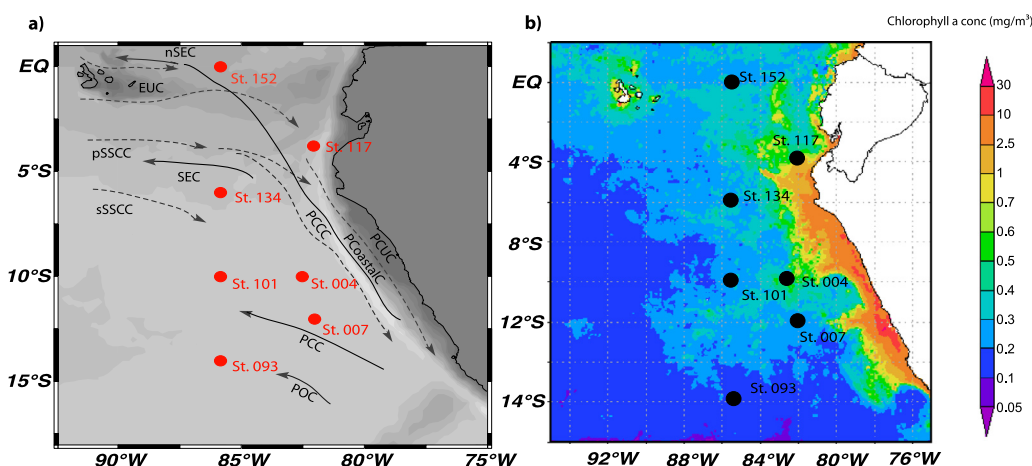


Fig. 1. (a) Station map of sampling locations and schematic surface (solid grey lines) and subsurface currents (dashed grey lines) off Ecuador and Peru according to Strub et al. (1998), Penven et al. (2005), Kessler (2006), Ayon et al. (2008), Karstensen and Ulloa (2008), and ADCP data according to Czeschel et al. (2011) (nSEC: northern South Equatorial Current, EUC: Equatorial Undercurrent, SEC: South Equatorial Current, pSSCC: primary Southern Subsurface Countercurrent, sSSCC: secondary Southern Subsurface Countercurrent, PCUC: Peru–Chile Undercurrent, PCC: Peru–Chile Current, PCCC: Peru–Chile Countercurrent, POC: Peru–Oceanic Current); (b) averaged Austral summer (Jan.–Feb. 2009) surface water distribution of Chl α concentration (mg/m³). Satellite data (MODIS Aqua) is adapted from NASA Giovanni (<http://disc.sci.gsfc.nasa.gov/giovanni/overview/index.html>).

isotopes to seawater. These processes can have an effect on the $\delta^{30}\text{Si}(\text{OH})_4$ in seawater, in particular in near surface waters given that most of the biogenic silica (bSiO₂) formed in the euphotic zone has been remineralized many times in the uppermost water column while on average only 3% of the bSiO₂ production is finally buried on the sea floor (Tréguer et al., 1995). The dissolution of bSiO₂ is strongly influenced by physical parameters, such as temperature and pH (Lewin, 1961), but bacterial activity, which destroys the protecting organic material surrounding the diatom frustules, can lead to enhanced dissolution rates (Bidle and Azam, 1999; Bidle et al., 2002), in particular in waters with high bacterial activities such as OMZs. A study by Beucher et al. (2011) in the Eastern Equatorial Pacific (EEP) also documented low $\delta^{30}\text{Si}(\text{OH})_4$ values in a zone of net silica dissolution and high biogenic silica content.

Currently it is unclear if the dissolution of sediments with high biogenic silica (bSiO₂) also has an effect on the $\delta^{30}\text{Si}(\text{OH})_4$ distribution in deep water masses. Several studies have shown that the $\delta^{30}\text{Si}(\text{OH})_4$ signatures of deep water masses are characterized by distinct Si isotope signatures (e.g. Cardinal et al., 2005; Reynolds et al., 2006; Beucher et al., 2008; De Souza et al., 2012a), despite that earlier model results suggested that no variation of the $\delta^{30}\text{Si}(\text{OH})_4$ in deep waters is expected (Wischmeyer, 2003). A study by Reynolds et al. (2006) in the North Pacific revealed low $\delta^{30}\text{Si}(\text{OH})_4$ signatures for North Pacific Deep Water (NPDW, +0.6‰), whereas Circumpolar Deep Water (CDW) in the Southern Ocean has values around +1.2‰ (Cardinal et al., 2005; De Souza et al., 2012b). However, new data by De Souza et al. (2012b) suggested that this heterogeneity may rather reflects analytical uncertainties and that thus no clear trends in the deep Pacific can be observed as a consequence of water mass mixing and dissolution processes. This important issue can only be resolved by a systematic coverage of different areas in the Pacific Ocean with high quality data.

In this study we analyzed the dissolved stable Si isotope composition of 7 full water column stations in the Eastern Equatorial Pacific (EEP) offshore the Peruvian upwelling area, for which to date no data have been available. The main goal of the study is a better understanding of the influence of the biogeochemical cycling of silicate and its relationship to the pronouncedly low oxygen concentrations on the distribution of the $\text{Si}(\text{OH})_4$ concentrations and their corresponding Si isotope compositions. Furthermore the

Si isotope distribution in deep waters of the Pacific Ocean is targeted in order to investigate possible sources.

2. Material and methods

2.1. Sampling and chemical preparation

All samples were collected during cruises M77-3 and M77-4 with the German RV Meteor in the frame of the Collaborative Research Centre (SFB) 754: Climate–Biogeochemistry Interactions in the Tropical Ocean between December 2008 and February 2009. Seawater samples were collected along two meridional sections at 85°50'W and 82°00'W off the Ecuadorian and Peruvian coasts between the equator and 14°S (Fig. 1, Table 1).

Seawater samples for analysis of Si isotope, nutrient and oxygen concentration measurements were collected using a Seabird CTD Rosette System equipped with an oxygen sensor. Nutrient concentrations were measured following Grasshoff et al. (1999). Oxygen concentrations were determined with the O₂-sensor of the CTD and were later calibrated with bottle data obtained by Winkler titration (Winkler, 1888). Seawater samples for Si isotope measurements were immediately filtered through nitrocellulose acetate filters (0.45 µm pore size) on board and were then acidified with distilled concentrated HCl to pH 2 because aliquots of these samples were also used for Rare Earth Element analyses. At GEOMAR the Si was separated from the samples using a brucite-coprecipitation method, the so called MAGIC method (Reynolds et al., 2006; after Karl and Tien, 1992). Between 5 and 300 ml of seawater were used depending on the Si concentration. Only samples with yields > 98% (determined photometrically) were used for isotopic measurements given that incomplete precipitation leads to fractionation of the Si contained in the samples. Samples with $\text{Si}(\text{OH})_4$ below 10 µmol/L were preconcentrated through repeated precipitation steps applying the same method. For this purpose, the brucite precipitate was redissolved in HCl (pH 2) and an additional preconcentration step was performed, for which again approximately 1% v/v of 1 M NaOH were added. Each precipitation step leads to the precipitation of approximately 10% of the magnesium contained in the water samples, but redissolution after precipitation reduced the Mg content in the sample solution significantly. Preconcentration was necessary to ensure that ~ 70 nmol Si were processed through ion-exchange chromatography (see also Reynolds et al., 2006; Ehlert et al., 2012).

Table 1

Sampling locations with silicon isotope data ($\delta^{30}\text{Si}(\text{OH})_4$), nutrient concentrations as well salinity, potential temperature and potential density. External errors are given in 2σ standard deviation for the sample-bracketing method ($2\sigma_{\text{sd smp. brack}}$) as well as for n duplicate measurements on different days given as ($2\sigma_{\text{sd repeated}}$).

	Depth (m)	$\delta^{30}\text{Si}$ (‰)	n	$2\sigma_{\text{sd smp}}$ brack.	$2\sigma_{\text{sd}}$ repeated	Pot. temp. (°C)	Neutr. density (kg/m ³)	Salinity (PSS)	Si(OH) ₄ (μmol/kg)	Si* (μmol/kg)	NO ₃ ⁻ (μmol/kg)	PO ₄ ⁻ (μmol/kg)	Oxygen (μmol/kg)
M77-3	2	2.62	2	–	0.43	24.10	23.78	35.22	0.69	–4.59	5.28	0.68	213.81
St. 004	21	2.13	1	0.16	–	21.54	24.54	35.23	3.47	–8.60	12.07	1.23	206.78
10°S/82°30'W	41	1.81	1	0.23	–	15.27	25.97	35.02	14.59	–16.11	30.70	2.54	10.56
4444 m depth	60	1.56	1	0.23	–	14.31	26.16	35.00	16.33	–13.40	29.73	2.52	2.37
	92	1.58	3	–	0.30	13.49	26.31	34.96	19.81	–9.08	28.89	2.59	2.05
	201	1.83	2	–	0.22	12.40	26.49	34.90	22.24	–11.53	33.77	2.57	4.24
	250	1.47	2	–	0.17	11.82	26.58	34.86	24.32	–7.96	32.28	2.61	2.19
	328	1.39	2	–	0.06	10.98	26.70	34.81	27.10	–6.57	33.67	2.82	2.31
	502	1.39	2	–	0.08	8.59	27.01	34.65	33.36	–10.51	43.87	3.01	6.61
	999	1.18	2	–	0.11	4.38	27.55	34.55	69.17	20.04	49.13	3.27	52.65
	1802	0.92	4	–	0.24	2.37	27.86	34.64	77.85	33.26	44.59	2.89	92.63
M77-3	2	2.96	2	–	0.06	24.15	23.92	35.41	0.69	–5.85	6.54	0.85	215.17
St. 007	30	1.94	2	–	0.32	17.80	25.51	35.21	4.86	–6.49	11.35	1.53	219.23
12°S/81°W	60	1.48	1	0.13	–	14.55	26.06	34.94	20.85	1.86	18.99	2.95	4.26
4749 m depth	70	1.61	1	0.12	–	14.09	26.18	34.96	22.58	8.18	14.40	2.96	2.39
	100	1.42	3	–	0.28	13.41	26.32	34.95	27.80	22.22	5.58	2.93	1.94
	199	1.39	1	0.19	–	12.50	26.47	34.90	27.45	12.62	14.83	2.95	2.06
	499	1.50	1	0.17	–	8.38	27.01	34.62	32.32	–12.41	44.73	3.28	7.83
	999	1.06	1	0.25	–	4.27	27.56	34.54	66.04	17.35	48.69	3.32	53.22
	1499	1.11	1	0.11	–	2.95	27.77	34.60	76.81	30.42	46.39	3.24	78.00
	1800	1.15	2	–	0.17	2.37	27.87	34.6341	125.81	81.22	44.59	2.99	92.15
M77-4	3	4.36	3	–	0.04	24.72	23.83	35.52	0.22	–3.50	3.72	0.53	221.17
St. 093	50	1.43	1	0.18	–	20.19	25.03	35.40	1.51	–4.48	5.99	0.78	240.80
14°S/85°50'W	101	1.96	2	–	0.13	16.51	25.66	35.00	1.69	–7.37	9.06	1.06	194.84
4579 m depth	150	1.17	1	0.23	–	13.23	26.26	34.83	18.89	–2.26	21.15	2.68	18.27
	174	1.22	2	–	0.18	12.55	26.40	34.83	24.00	6.00	18.00	2.74	2.94
	1007	1.28	3	–	0.05	4.31	27.55	34.54	79.50	35.42	44.08	3.19	57.98
	2003	1.13	4	–	0.07	2.17	27.90	34.64	130.85	91.20	39.65	2.87	105.82
	3004	1.14	3	–	0.23	1.59	28.00	34.68	138.71	101.13	37.58	2.66	132.76
	4036	1.04	4	–	0.24	1.44	28.04	34.69	127.87	92.37	35.50	2.52	153.06
M77-4	3	2.57	2	–	0.17	26.06	23.37	35.47	1.20	–2.43	3.63	0.45	215.54
St. 101	50	2.01	2	–	0.10	18.62	25.27	35.18	3.54	–8.07	11.61	1.19	168.45
10°S/85°50'W	101	1.87	1	0.08	–	13.76	26.26	34.97	18.20	–9.44	27.64	2.38	6.06
4420 m depth	152	1.88	1	0.17	–	12.70	26.44	34.91	24.10	NaN	NaN	NaN	5.32
	502	1.77	1	0.10	–	8.33	27.04	34.63	40.30	NaN	NaN	NaN	4.65
	1503	1.37	3	–	0.32	2.77	27.80	34.61	118.06	76.64	41.42	2.98	89.22
M77-4	2	2.32	2	–	0.19	22.53	23.66	34.46	2.69	–4.98	7.67	0.74	195.24
St. 117	31	1.72	1	0.22	–	15.71	25.93	35.11	12.69	–9.15	21.84	1.62	77.01
3°35'W/82°W	75	1.42	3	–	0.23	14.48	26.14	35.01	16.43	–9.93	26.36	1.93	50.20
4085 m depth	100	1.75	1	0.22	–	14.19	26.19	34.99	17.41	–9.84	27.25	1.98	43.19
	151	1.42	2	–	0.23	13.63	26.29	34.96	19.18	–7.77	26.95	1.97	47.08
	401	1.52	2	–	0.05	9.06	26.97	34.69	41.61	2.75	38.86	2.9	6.05
	1501	1.04	2	–	0.01	3.09	27.76	34.61	121.07	80.43	40.64	2.99	79.61
	2501	1.16	2	–	0.04	1.75	27.98	34.67	145.60	107.72	37.88	2.75	116.68
	3501	1.13	4	–	0.14	1.52	28.02	34.68	143.63	107.13	36.50	2.64	132.62
M77-4	2	2.19	2	–	0.26	26.90	22.29	34.39	1.52	–2.66	4.18	0.39	218.81
St. 134	51	1.69	2	–	0.32	15.73	25.88	35.05	3.37	–7.15	10.52	0.96	41.60
6°S/85°50'W	100	1.61	1	0.13	–	13.83	26.26	34.98	18.20	–10.62	28.82	2.09	28.77
4103 m depth	199	1.58	1	0.16	–	12.77	26.43	34.92	21.25	–10.13	31.38	2.35	7.43
	400	1.26	2	–	0.04	9.43	26.90	34.71	32.46	–0.20	32.66	2.77	3.21
	751	1.41	1	–	0.12	5.77	27.37	34.56	63.34	18.91	44.43	3.21	34.78
	4002	1.23	5	–	0.18	1.50	28.03	34.68	141.66	104.27	37.39	2.66	136.49
M77-4	3	2.39	2	–	0.24	26.06	21.97	33.61	1.69	–2.58	4.27	0.49	212.23
St. 152	20	1.80	1	0.13	–	18.36	25.17	34.95	7.22	–7.93	15.15	1.22	139.21
Equator/85°50'W	51	1.57	1	0.09	–	14.75	26.08	35.02	14.06	–6.50	20.56	1.54	92.41
2906 m depth	90	1.47	3	–	0.24	14.03	26.22	34.98	16.00	NaN	NaN	NaN	87.72
	150	1.62	1	0.20	–	13.74	26.26	34.97	18.00	–6.79	24.79	1.86	62.26
	199	1.58	1	0.15	–	12.76	26.42	34.90	22.13	–6.79	28.92	2.12	39.49
	398	1.65	2	–	0.02	9.42	26.91	34.71	39.55	2.16	37.39	2.83	7.57
	598	1.30	2	–	0.10	7.23	27.20	34.61	52.83	12.19	40.64	3	26.40
	999	1.24	6	–	0.24	4.68	27.53	34.57	85.99	44.76	41.23	3.06	62.58
	2500	1.23	2	–	0.14	1.88	27.96	34.67	152.49	114.12	38.37	2.84	106.01

For Si isotope measurements the samples were purified via column chemistry following the method by Georg et al. (2006) as modified by De Souza et al. (2012a) and were measured on a Nu-Plasma HR MC-ICPMS (Nu instruments) at GEOMAR. The MC-ICPMS is equipped with an adjustable source-defining slit set to medium resolution to ensure separation of the ^{30}Si peak from molecular interferences. Measurements were carried out with a standard-sample bracketing method (Albarède et al., 2004). All solutions were measured at a Si concentration of 14 to 21 $\mu\text{mol/kg}$ depending on the performance of the instrument and were introduced into the plasma via a Cetac Aridus II desolvator equipped with a PFA nebulizer with an uptake rate of 60 to 80 $\mu\text{L/min}$.

Si isotope compositions are reported in the δ -notation using the reference standard NBS28 in parts per thousand ($\delta^{30}\text{Si} = ((R_{\text{sample}}/R_{\text{standard}}) - 1) \times 1000$), where R_{sample} is the $^{30}\text{Si}/^{28}\text{Si}$ ratio of the sample and R_{standard} is the $^{30}\text{Si}/^{28}\text{Si}$ ratio of the standard. External reproducibility is given as 2σ standard deviations either from the sample-bracketing method ($2\sigma_{\text{smp. brack.}}$) or the 2σ standard deviations of the mean $\delta^{30}\text{Si}$ value obtained on different measurement days ($2\sigma_{\text{sdrepeated}}$, Table 1). The external errors ($2\sigma_{\text{sd}}$) for the sample bracketing, where samples were measured 5 times range from 0.01‰ to 0.25‰. Samples measured on different days showed slightly higher errors ranging from 0.01 to 0.43. Long term repeated measurements of the reference materials IRMM018 and Big Batch gave average $\delta^{30}\text{Si}$ values of $-1.59 \pm 0.12\text{‰}$ ($2\sigma_{\text{sd}}$, $n = 25$) and $-10.75 \pm 0.20\text{‰}$ ($2\sigma_{\text{sd}}$, $n = 25$), respectively, which are in good agreement with values obtained by other laboratories (Reynolds et al., 2007). An internal seawater matrix standard gave a long-term external reproducibility of 0.2‰ ($2\sigma_{\text{sd}}$, $n = 15$). In all figures the error bar represents this long-term reproducibility. Samples with higher analytical uncertainties are marked.

2.2. Hydrographic setting of the study area

In the EEP, persistent easterly trade and alongshore winds produce offshore Ekman transport of surface waters, which are replaced by upwelling of nutrient-rich subsurface waters along the shelf. The main source water masses for the Peruvian upwelling are the southward flowing Peru–Chile Countercurrent (PCCC) and the Peru–Chile Undercurrent (PCUC, Brink et al., 1983). Surface waters of the sampling locations are mainly influenced by currents from the South or currents that are transported offshore from the shelf, such as the Peru–Oceanic Current (POC), the Peru–Coastal Current (PCoastalC) or the Peru Chile Current (PCC) (Fig. 1a, Strub et al., 1998; Penven et al., 2005; Karstensen and Ulloa, 2008). These currents are the driving force for the Equatorial Undercurrent (EUC), the Southern Subsurface Countercurrent (SSCC) as well as the South Equatorial Countercurrent (SECC) to flow eastward along the equator thereby supplying oxygen-rich waters to the upwelling area (Brink et al., 1983; Toggweiler et al., 1991; Fiedler and Talley, 2006). During Austral summer 2009, when the samples for this study were taken, the EUC was located at approximately 0°N to 1°N at a core depth of 90 m (Czeschel et al., 2011), almost exactly at the location of station 152 (Fig. 1a). Another water mass influencing the EEP is the Subantarctic Mode Water (SAMW). SAMW as well as Antarctic Intermediate Water (AAIW) are subducted surface waters formed in the eastern Pacific sector of the Southern Ocean, which transport water depleted in $\text{Si}(\text{OH})_4$ to the EEP and therefore can also be traced by their low Si^* properties ($\text{Si}^* = [\text{Si}(\text{OH})_4] - [\text{NO}_3^-]$), whereas more negative Si^* values are consequence of a depletion in $\text{Si}(\text{OH})_4$ compared to NO_3^- (Sarmiento et al., 2004; Aoki et al., 2007; Salée et al., 2010). According to Tsuchiya and Talley (1998) the core SAMW only extends to 28°S along 88°W . The southernmost stations (St. 101 & 93) of our study area show a salinity minimum

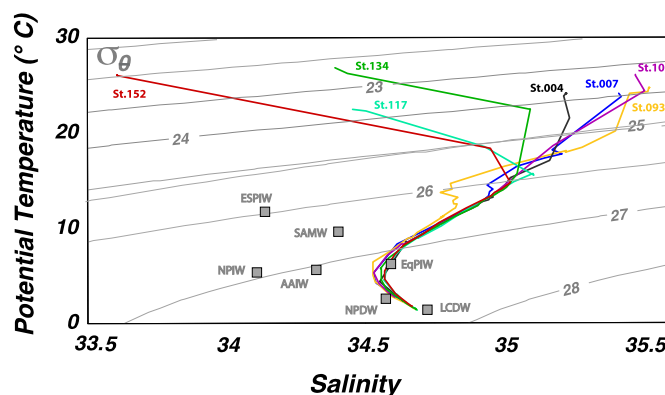


Fig. 2. T - S diagram with potential density isolines (σ_θ) for the 7 stations and corresponding water masses in the study area according to McCartney (1977), Johnson and Toole (1993), Tsuchiya and Talley (1998), Schneider (2003), Bostock et al. (2010), and Amakawa et al. (2009). LCDW: Lower Circumpolar Deep Water ($\sigma_\theta = 0.85$, Sal. 34.7), NPDW: North Pacific Deep Water ($27.6 < \sigma_\theta < 27.8$, $1^\circ\text{C} < T_{\text{pot.}} < 1.8^\circ\text{C}$; $3-5$, $34.6 < \text{Sal.} < 34.7$), NPIW: North Pacific Intermediate Water ($\sigma_\theta = 26.8$, $T_{\text{pot.}}: 6.4$, $33.9 < \text{Sal.} < 34.1$), AAIW: Antarctic Intermediate Water ($\sigma_\theta = 27.1$, $3^\circ\text{C} < T_{\text{pot.}} < 5^\circ\text{C}$, $34.3 < \text{Sal.} < 34.5$), EqPIW: Equatorial Pacific Intermediate Water ($\sigma_\theta = 27.3$, $34.5 < \text{Sal.} < 34.6$), SAMW: Subantarctic Mode Water ($\sigma_\theta = 26.5-27.1$, $T_{\text{pot.}} 4-15^\circ\text{C}$, Sal. $34.2-35.8$), ESPIW ($25.75 < \sigma_\theta < 26.2$, $11^\circ\text{C} < T_{\text{pot.}} < 13^\circ\text{C}$, $34.1 < \text{Sal.} < 34.3$). For a compilation of the displayed water mass properties, see also Grasse et al. (2012).

(34.8) at a water depth of 100 m to 170 m (Fig. 2), which corresponds to a potential density of about 26 kg/m^3 and is thus lower than SAMW (26.5 to 27.1 kg/m^3). Schneider (2003) described the salinity minimum in the EEP as Eastern South Pacific Intermediate Water (ESPIW, 26 kg/m^3). According to these authors the ESPIW is also a tongue of subducted low salinity water, which has its origin in the eastern South Pacific, similar to SAMW as described by McCartney (1977) and Tsuchiya and Talley (1998). As both water masses have their origin in the south, we will use the term modified SAMW (mSAMW) for the low salinity tongue.

Intermediate water of the EEP is mainly influenced by three water masses (Bostock et al., 2010 and references therein): North Pacific Intermediate Water (NPIW), Antarctic Intermediate Water (AAIW) and the Equatorial Pacific Intermediate Water (EqPIW) with potential densities ranging between 26.8 and 27.1 kg/m^3 . NPIW and AAIW are not clearly distinguishable based on their T - S properties, but NPIW generally shows higher $\text{Si}(\text{OH})_4$ concentrations between 50 and $130 \mu\text{mol/kg}$ compared to AAIW, which is characterized by concentrations between 5 and $80 \mu\text{mol/kg}$ (Bostock et al., 2010). AAIW is primarily formed in the southeast Pacific off the coast of southern Chile where it is subducted and flows northward to a latitude of approximately 20°S to 14°S (Wijffels, 1993; Talley, 1999; Kawabe and Fujio, 2010), whereas NPIW is formed in the northwestern subtropical gyre along the Kuroshio and Oyashio Front (Talley, 1999) and is generally characterized by lower oxygen concentrations ($150 \mu\text{mol/kg}$) than its Southern Hemisphere counterpart, the AAIW ($200-300 \mu\text{mol/kg}$, Table 1; Bostock et al., 2010). NPIW is detectable to approximately 20°N (Fiedler and Talley, 2006). Intermediate waters in the study area (between the Equator and 14°S) are dominated by EqPIW (Wijffels, 1993; Bostock et al., 2010).

In addition to the above currents, mesoscale eddies are a common feature in the Peruvian upwelling area and can influence the surface waters, as well as subsurface and intermediate waters (Chaigneau et al., 2009). They supply nutrients offshore and can be traced via satellite by the distribution of $\text{Chl } \alpha$ concentrations (Fig. 1b). Eddies therefore can have a major influence on biogeochemistry and the distribution and dynamics of marine ecosystems (Sweeney et al., 2003; Ganachaud et al., 2011; Altabet et al., 2012). During sampling time an anticyclonic eddy

with an inner diameter of approximately 300 km was located between 9°S and 13°S. The centre of the eddy was near 11°S and 80°30'W (Fig. 1b and Fig. 4b).

The densest water mass in the Pacific basin is Lower Circumpolar Deep Water (LCDW) (Wijffels et al., 1996), which is also formed in the Southern Ocean and then flows northward along different pathways. Through internal mixing processes LCDW is transformed into North Pacific Deep Water (NPDW), which is again modified by admixture of Upper Circumpolar Deep Water (UCDW) near the Hawaiian Islands. From there NPDW broadly flows southward along the continental slope of Central and South America and contributes to the mixture of deep waters off Peru (Wijffels et al., 1996; Kawabe and Fujio, 2010). The deep water masses, like NPDW and LCDW show only small differences in their hydrographic properties but NPDW can be distinguished on the basis of its significantly higher silicate concentrations and lower oxygen concentrations than those of LCDW.

3. Results

3.1. Si isotope distribution in the water column

Water column data show a general decrease of $\delta^{30}\text{Si}(\text{OH})_4$ with increasing $\text{Si}(\text{OH})_4$ concentrations (Fig. 3). The $\text{Si}(\text{OH})_4$ concentrations increase at all stations from low values in the surface waters (minimum at 0.22 $\mu\text{mol/kg}$) to high concentrations (maximum at 153 $\mu\text{mol/kg}$) in deep waters (Figs. 3 and 4, Table 1). This pattern is generally reflected by the corresponding Si isotope compositions and the highest $\delta^{30}\text{Si}(\text{OH})_4$ values are systematically found in the surface waters (Fig. 4). For a better comparison offshore stations (solid squares) are plotted together with the nearshore stations (open squares) for similar latitudes from north to south (Fig. 3). In general there are no large differences in $\text{Si}(\text{OH})_4$ and $\delta^{30}\text{Si}(\text{OH})_4$ between the offshore and the nearshore stations. Nearshore stations (St. 4 & 7) from 10°S to 14°S show slightly lower $\text{Si}(\text{OH})_4$ at water depths between 328 and 1800 m compared to the offshore stations (St. 101 & 93). The slightly higher $\text{Si}(\text{OH})_4$ concentrations at offshore station 101 is mirrored by rather high $\delta^{30}\text{Si}(\text{OH})_4$ values (+1.7‰ to +1.4‰) at similar depths in contrast to lighter $\delta^{30}\text{Si}(\text{OH})_4$ values at station 4 (+1.4‰ and +0.9‰) (Fig. 3).

Deep water $\text{Si}(\text{OH})_4$ concentrations increase continuously to a depth of approximately 2000 m and below remain essentially constant at values near 140 $\mu\text{mol/kg}$. While the silicic acid concentrations increase with depth the $\delta^{30}\text{Si}(\text{OH})_4$ signatures at the same time remains remarkably constant. The lowest $\delta^{30}\text{Si}(\text{OH})_4$ values in deep waters are observed at stations 4 ($\delta^{30}\text{Si}(\text{OH})_4 = +0.9 \pm 0.2\text{‰}$, 1800 m) and 93 ($\delta^{30}\text{Si}(\text{OH})_4 = +1.0 \pm 0.2\text{‰}$, 4036 m), whereas the stations further north (St. 134, 6°S and St. 152, equator) show a slightly higher $\delta^{30}\text{Si}(\text{OH})_4$ signature of $+1.2 \pm 0.1\text{‰}$ at 4000 m depth (Fig. 3). Considering an external reproducibility, these values are, however, not significantly different from each other. Waters below 2000 m show an overall mean of $+1.2 \pm 0.2\text{‰}$ ($n = 7$, 1sd).

3.2. Si isotope distribution in surface waters

The $\delta^{30}\text{Si}(\text{OH})_4$ signatures of the surface waters range from +2.2‰ to +4.4‰ (Fig. 4a, Table 1). Fig. 4a shows a comparison to $\delta^{30}\text{Si}(\text{OH})_4$ data adapted from Ehlert et al. (2012). The highest $\delta^{30}\text{Si}(\text{OH})_4$ values of +3.0‰ and +4.4‰ are found at stations 7 and 93 in the south of the study area. Surface samples north of 10°S are rather homogeneous in their $\delta^{30}\text{Si}(\text{OH})_4$ signatures ranging between +2.2‰ and +2.6‰, corresponding to $\text{Si}(\text{OH})_4$ concentrations between 0.7 and 2.7 $\mu\text{mol/kg}$. The $\delta^{30}\text{Si}(\text{OH})_4$ distribution in the surface waters generally display a trend from low $\delta^{30}\text{Si}(\text{OH})_4$ values in the north to high values in the south. Surface waters along the Ecuadorian and Peruvian shelf (data adapted

from Ehlert et al., 2012) range between +1.7‰ and +2.8‰. Between approximately 9°S and 13°S an anticyclonic eddy influenced the study area. The extent of the eddy can clearly be identified by satellite derived chlorophyll α (Chl α) data (Fig. 1b), as well as the altimeter-derived sea level anomaly (SLA) data (Fig. 4b, Czeschel et al., 2011).

3.3. Subsurface and intermediate water masses in the OMZ

Fig. 5a shows the distribution of $\delta^{30}\text{Si}(\text{OH})_4$ for the upper 500 m (surface samples not shown) of the 85°50'W transect in comparison to Si^* values. The most negative values of Si^* ($\sim -10 \mu\text{mol/kg}$) occur at approximately 60 m to 200 m depth between 14°S and 2°30'S (St. 101 & 134), corresponding to $\delta^{30}\text{Si}(\text{OH})_4$ of +1.5‰ to +1.9‰. Negative Si^* values at station 93 (100 m) correspond to high $\delta^{30}\text{Si}(\text{OH})_4$ values (+1.9‰), whereas waters with a positive Si^* (5 $\mu\text{mol/kg}$) consistently show lower values of +1.2‰ (150 m and 170 m). Fig. 5b shows the corresponding oxygen concentrations (contour lines) and N:P ratios (color shading) along the 85°50'W transect. The OMZ (characterized by oxygen concentrations below 10 $\mu\text{mol/kg}$) in the study area extends between 50 and 300 m water depth for the upper boundary and between 370 and 500 m depth for the lower boundary (Fig. 5b, Table 1). Samples along the 85°50'W transect are influenced by currents from the Central Pacific, such as the SEC and the EUC, which are characterized by elevated oxygen concentrations, as well as by currents flowing westward, such as the SECC and the SSCC (Fig. 5b). Samples within the OMZ show the largest Si isotopic range even along the same density surfaces (Fig. 6). Between a neutral density (γ^n) of 26.25 and 27 kg/m^3 the Si isotope signatures range between +1.1‰ and +1.9‰ although the $\text{Si}(\text{OH})_4$ varies only slightly for these same samples.

4. Discussions

4.1. Silicic acid utilization in and water mass transport in surface waters

The surface water $\delta^{30}\text{Si}(\text{OH})_4$ in the study area ranges from +2.2‰ to +4.4‰ with the highest values occurring at the southernmost stations (St. 93; 14°S & 7; 12°S, Fig. 4). The dissolved $\text{Si}(\text{OH})_4$ in surface waters is fractionated during utilization of silicic acid, mainly by diatoms. Apart from utilization the dissolved $\delta^{30}\text{Si}(\text{OH})_4$ signal is influenced by mixing of water masses (Reynolds et al., 2006; Fripiat et al., 2011).

The value of +4.4‰ at the surface of St. 93 is the highest measured $\delta^{30}\text{Si}(\text{OH})_4$ observed so far for seawater and corresponds to an extremely depleted $\text{Si}(\text{OH})_4$ concentration of 0.2 $\mu\text{mol/kg}$ (Fig. 4, Table 1). Station 93 is clearly influenced by the POC a water mass originating from the southeast (Figs. 1 and 5b, Czeschel et al., 2011). The $\text{Si}(\text{OH})_4$ concentration of the POC gets strongly depleted while flowing along the high productivity areas off the Chilean coast (Daneri et al., 2000). For comparison, Reynolds et al. (2006) observed $\delta^{30}\text{Si}(\text{OH})_4$ of +3.2‰ in oligotrophic surface waters of the subtropical gyre in the North Pacific corresponding to a $\text{Si}(\text{OH})_4$ concentration of 0.6 $\mu\text{mol/kg}$. Similar Si isotope values in surface waters of the Eastern Pacific (60°S) were also measured by De Souza et al. (2012b), who found +3.2‰ at relatively elevated concentrations of 6.3 μM . A recent modeling study by Matsumoto et al. (2013) also estimated possible $\delta^{30}\text{Si}(\text{OH})_4$ values around +4‰ in oligotrophic regions. The study by Ehlert et al. (2012) along the Peruvian shelf, which is characterized by pronounced coastal upwelling, showed that strong upwelling leads to significantly less fractionated surface waters (Fig. 4a). Surface waters along the shelf are characterized by Si isotope values ranging from +1.7‰ to +2.8‰, whereby the least fractionated surface waters were found between 5°S and 15°S corresponding to the

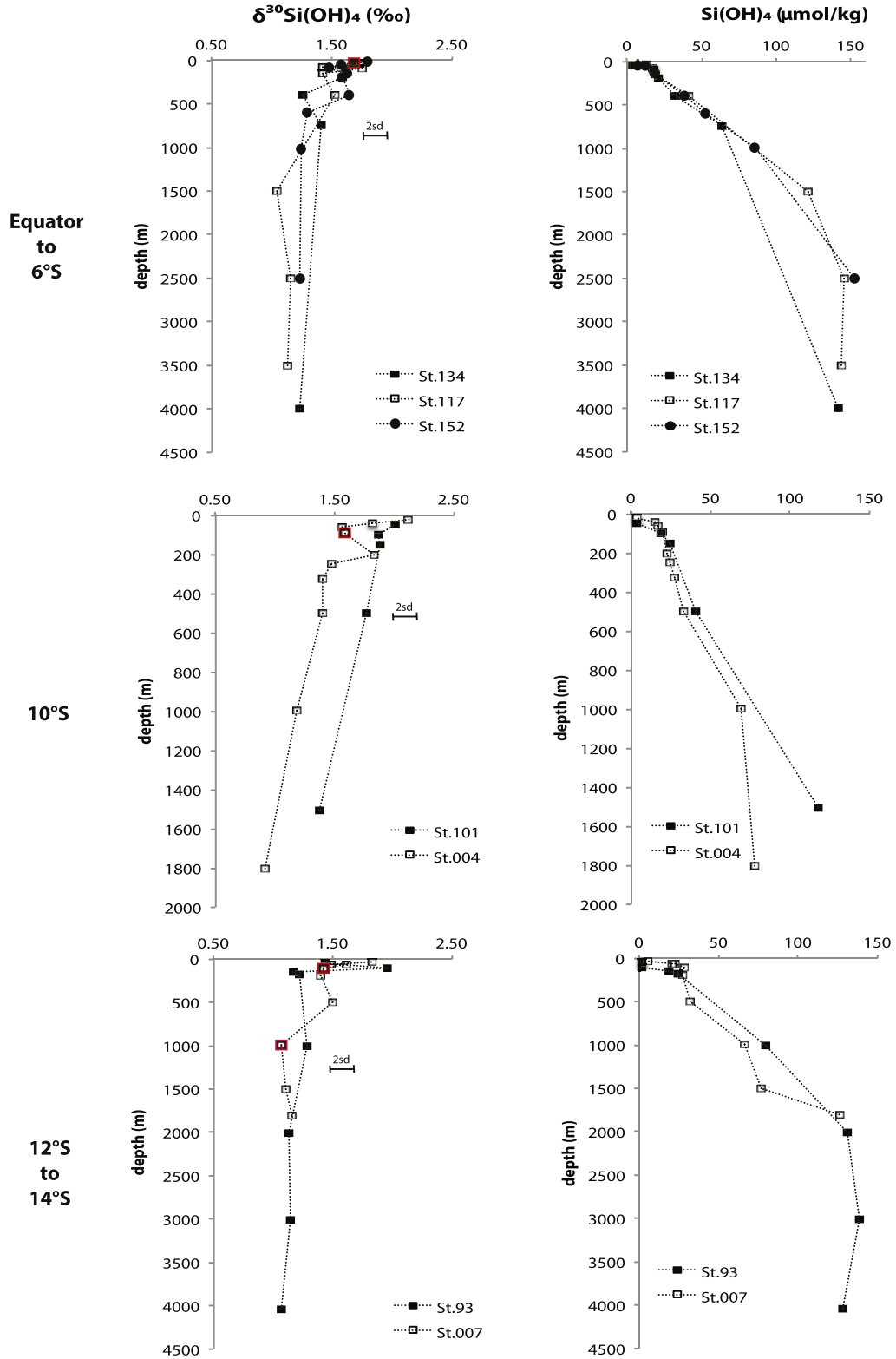


Fig. 3. Water column profiles for $\delta^{30}\text{Si}(\text{OH})_4$ signatures (left) and dissolved silicic acid concentrations in $\mu\text{mol/kg}$ (right) for the different stations sorted by latitude from north to south and distance from shore. Closed symbols mark the stations along the $85^\circ 50' \text{W}$ offshore transect (St. 134, 152, 101 & 93). Open symbols mark the stations near 82°W . For a better scaling the surface data are not shown here (see Fig. 4). Please, note the different depth range for stations at 10°S . The error bars in each figure represent the long-term error of the internal seawater matrix standard ($2\sigma_{\text{sd}}$). Samples with a higher error are marked in red (see Table 1). (For interpretation of the references to color in this figure legend, the reader is referred to the web version of this article.)

strongest upwelling. This isotopic signal of low fractionated surface waters are most likely transported offshore either via westward surface currents or via mesoscale eddies (Figs. 1 and 4). Fig. 1 shows the Chl α distribution in the study area, for which the

highest concentrations (up to 20 mg/m^{-2}) are found along the coast, indicating high primary productivity, mainly driven by diatoms under strong upwelling conditions (Franz et al., 2012). The Chl α distribution also marks the extent of the eddy. The off-

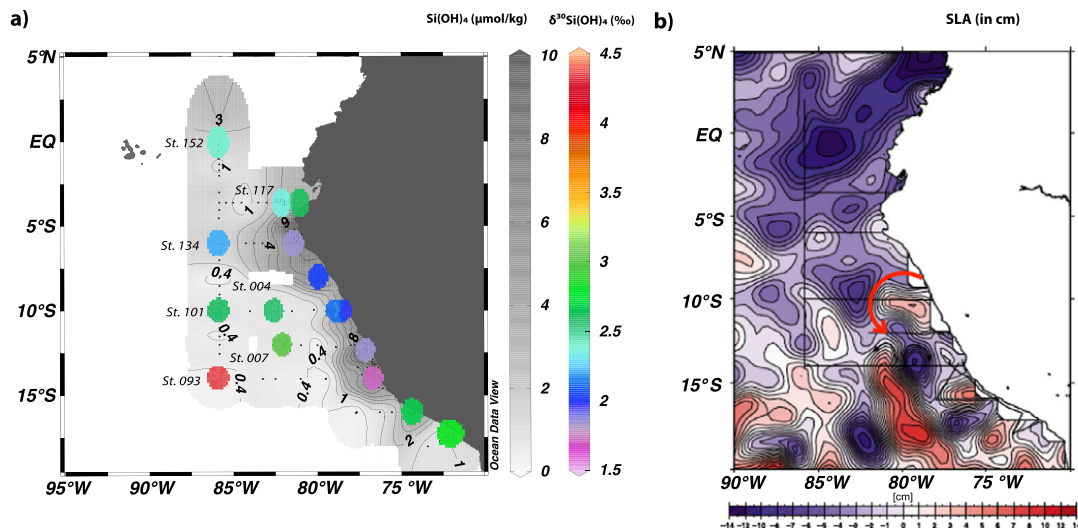


Fig. 4. (a) $\delta^{30}\text{Si}(\text{OH})_4$ distribution in surface waters ranging from +2.2‰ to +4.4‰ (in color) together with silicic acid concentrations (black contour lines and shading). The plot shows a compilation with data adapted from Ehlert et al. (2012) and (b) altimeter-derived sea level anomaly (SLA in cm) on 4 February 2009 (<http://www.aviso.oceanobs.com/>). CTD sections of cruises M77-3 and M7-4 are shown as black lines. The arrow indicates the anticyclonic eddy, which develops at the coast (see also Czeschel et al., 2011). (For interpretation of the references to color in this figure legend, the reader is referred to the web version of this article.)

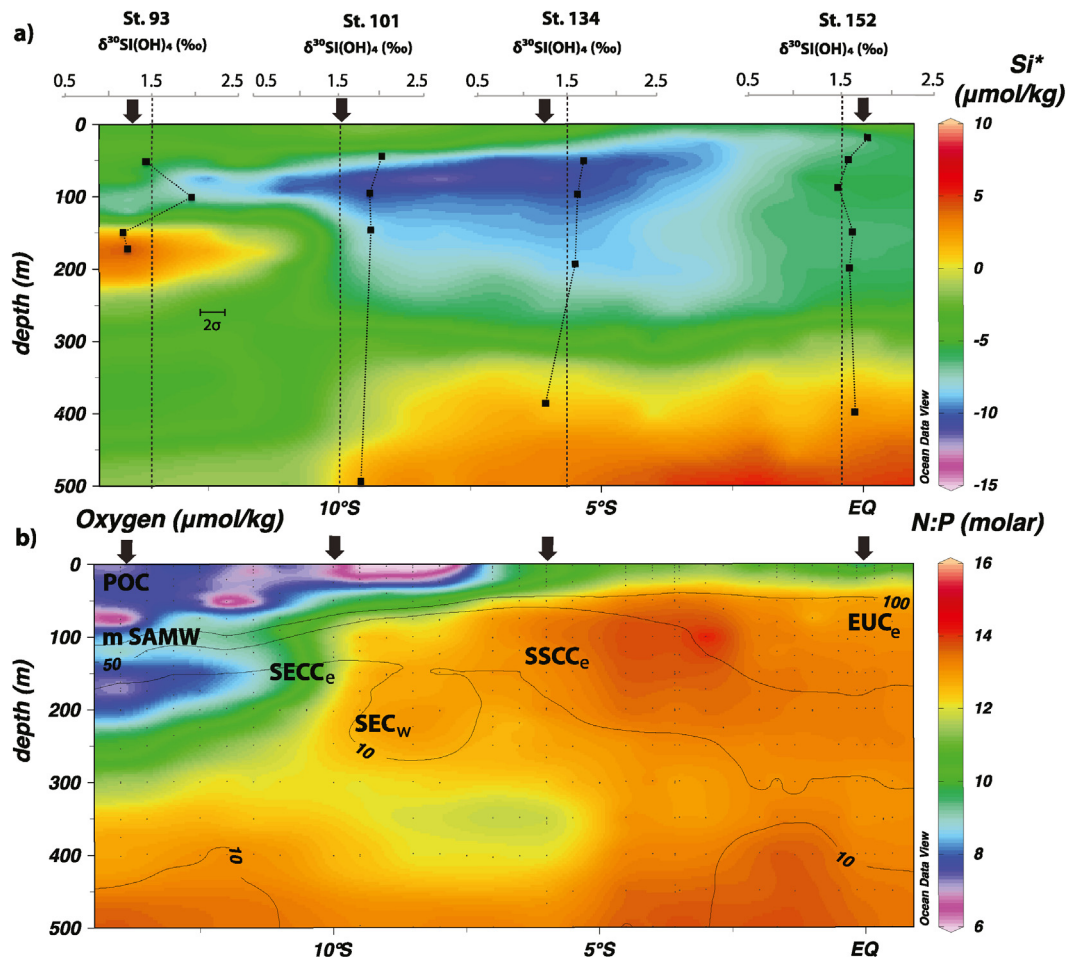


Fig. 5. (a) Si^* ($\text{Si}^* = [\text{Si}(\text{OH})_4] - [\text{NO}_3^-]$) distribution ($\mu\text{mol/kg}$) along the $85^\circ 50' \text{W}$ transect together with $\delta^{30}\text{Si}(\text{OH})_4$ (‰) profiles for the upper 500 m water depth. For a better scaling, the surface samples are not displayed. (b) Oxygen concentrations ($\mu\text{mol/kg}$) (contour lines) together with N:P ratios (color shading). The sampling location are marked by errors and for reference also $\delta^{30}\text{Si}(\text{OH})_4 = 1.5$ ‰ is indicated (dashed line). Surface and subsurface currents are indicated along the $85^\circ 50' \text{W}$ transect according to ADCP data (Czeschel et al., 2011). POC: Peru Oceanic Current, mSAMW: modified Subantarctic Mode Water, SSCC: Southern Subsurface Countercurrent, SECC: South Equatorial Countercurrent, SEC: South Equatorial Current, EUC: Equatorial Undercurrent. The flow direction eastward (e) or westward (w) is also indicated. Only the offshore transect is shown here given that insufficient nutrient and oxygen data are available for the nearshore transect.

shore transport of these waters has an influence on St. 4 and St. 7, which are located at the outer edge of the eddy. While St. 4 which

is located further north is characterized by Si isotope values of about +2.6‰, St. 7 marks the endpoint of the eddy filament and

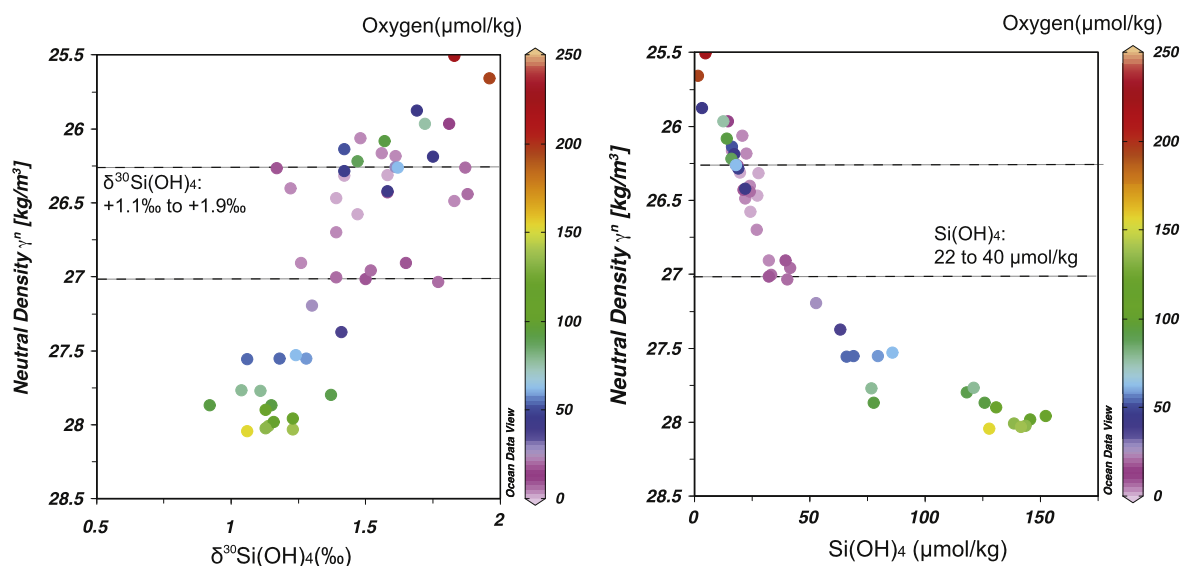


Fig. 6. (a) $\delta^{30}\text{Si}(\text{OH})_4$ (‰) and (b) silicic acid concentrations ($\mu\text{mol/kg}$) against neutral density γ^n (kg/m^3) ranging from 25.5 to 28.5 kg/m^3 corresponding to subsurface and intermediate water samples. The dashed lines indicate the density layer in which oxygen concentrations are mainly below 10 $\mu\text{mol/kg}$. The oxygen concentrations ($\mu\text{mol/kg}$) for the water samples are given in the color code. Note that not all surface samples are included. (For interpretation of the references to color in this figure legend, the reader is referred to the web version of this article.)

is characterized by highly fractionated $\delta^{30}\text{Si}(\text{OH})_4$ values ($+3\text{‰}$). Those large mesoscale eddies can therefore have a major influence on the dynamics of marine ecosystems (Sweeney et al., 2003; Ganachaud et al., 2011) and also influences biogeochemistry and the stable isotope distribution. A study by Altabet et al. (2012) already have shown that eddies have an influence on the N-cycle and the stable nitrogen isotopes. Surface waters of this study show a large range in Si isotope signatures, which is not only influenced by the degree of utilization but also strongly affected by surface currents also induced by eddies and upwelling intensity.

Until recently the widely applied enrichment factor (ε) of -1.1‰ determined in culture experiments has been considered diatom species independent (De la Rocha et al., 1997; Milligan et al., 2004), whereas recent investigations showed that ε is highly species dependent ranging from -0.5 to -2.1‰ , for polar and subpolar species (Sutton et al., 2013). Therefore the diatom assemblages might also have an influence on the $\delta^{30}\text{Si}(\text{OH})_4$ in surface water because the enrichment factors (Sutton et al., 2013). Diatom species cultured under strictly controlled conditions revealed that enrichment factors are species dependent and vary widely, at least for polar and subpolar species. For example culture studies with *Chaetoceros brevis* cultures show a Si isotope enrichment factor of about -2.1‰ , while *Fragilariopsis kerguelensis* only shows a enrichment factor of -0.5‰ (Sutton et al., 2013). However, even though the diatom assemblages in the coastal upwelling are dominated by *Chaetoceros* spp. (Abrantes et al., 2007; Hauss et al., 2012), we find even the lowest fractionated surface waters in this region suggesting that water mass mixing and nutrient re-supply exerts the main control on the Si isotope signature on the shelf.

4.2. Factors influencing $\delta^{30}\text{Si}(\text{OH})_4$ in subsurface water and intermediate waters of the OMZ

Subsurface and intermediate waters, characterized by neutral densities of $\gamma^n > 26.25 \text{ kg/m}^3$, show a large range in $\delta^{30}\text{Si}(\text{OH})_4$ ($+1.0\text{‰}$ to $+1.9\text{‰}$) (Figs. 6 and 7). Station 152 near the equator, which is clearly influenced by the incoming EUC at a depth of 90 m (Fig. 5b), shows a $\delta^{30}\text{Si}(\text{OH})_4$ of $+1.5 \pm 0.2\text{‰}$, which is in agreement to a study by Beucher et al. (2011) at 140°W , where the authors observed $\delta^{30}\text{Si}(\text{OH})_4$ of $+1.5\text{‰}$ for the EUC. In con-

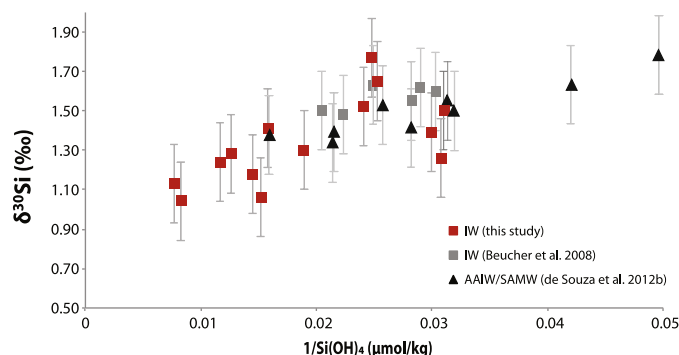


Fig. 7. $\delta^{30}\text{Si}(\text{OH})_4$ versus $1/\text{Si}(\text{OH})_4$ ($\mu\text{mol/kg}$) showing intermediate water (IW) samples with neutral density γ^n ranging from 26.8 to 27.4 kg/m^3 (water depth between 200 to 2000 m). Compilation of data adapted from Beucher et al. (2008, grey squares), de Souza et al. (2012b, black triangles) and this study (red squares). (For interpretation of the references to color in this figure legend, the reader is referred to the web version of this article.)

trast, another study by Beucher et al. (2008) at 110°W showed higher Si isotope values for the EUC of $+2.4\text{‰}$. The authors suggested that the high $\delta^{30}\text{Si}(\text{OH})_4$ signatures could be a result of the transport of highly fractionated surface waters from the subantarctic. However, the $\delta^{30}\text{Si}(\text{OH})_4$ distribution of the EUC in our study at $85^\circ 50'\text{W}$ is not distinctly different from other water masses in the EEP at similar water depths and more likely reflects the admixture of a water mass with lower Si isotope signature due to dissolution processes. Demarest et al. (2011) could show, that in the EEP at 140°W up to 52% of the bSiO_2 production is already re-dissolved within the upper 300 m (Demarest et al., 2011), whereby the dissolution of bSiO_2 is expected to result in lighter dissolved $\delta^{30}\text{Si}(\text{OH})_4$ signatures (Demarest et al., 2009). Stations 93 and 101 are influenced by mSAMW (Figs. 2 and 5). De Souza et al. (2012b) showed that SAMW and AAIW are traceable in the subtropical Pacific Ocean by their distinct isotopic signature ($+1.8\text{‰}$) in the subtropical ocean, even though the signal is not longer conserved in the equatorial region (at approximately $11^\circ 45'\text{S}$, 103°W). SAMW is a subducted surface water mass formed in the Southern Ocean, which has undergone utilization processes therefore carrying generally a negative Si^* of about $-18 \mu\text{mol/kg}$. As the SAMW flows

northward the Si^* increases to about $-6 \mu\text{mol/kg}$ (De Souza et al., 2012b). According to salinity properties, waters between 100 and 170 m at Station 93 show a salinity minimum (Fig. 2), but in our data set only the sample at 100 m depth actually shows the expected negative Si^* value ($-7 \mu\text{mol/kg}$, Fig. 5a). Samples from St. 93 at 150 and 170 m depth are characterized by higher Si^* values of -2.3 and $+6 \mu\text{mol/kg}$, respectively, whereby the more positive values can be explained by admixture of water masses originating from the shelf, which have undergone slight NO_3^- depletion within the OMZ. This is also reflected by low N:P ratios (~ 8) at these stations. In general N:P ratios in the open ocean are near 16:1 (Redfield, 1958), but due to different processes, such as N_2 fixation, N-loss, or remobilization of phosphate from the shelf sediments the ratio can be strongly biased. Low oxygen concentrations (2 to $10 \mu\text{mol/kg}$) for example induce N-loss processes, such as denitrification ($\text{NO}_3^- \rightarrow \text{NO}_2^- \rightarrow \text{NO} \rightarrow \text{N}_2\text{O} \rightarrow \text{N}_2$) and/or the more direct anammox process ($\text{NH}_4 + \text{NO}_2^- \rightarrow \text{N}_2$; Codispoti, 2007; Lam et al., 2009; Kalvelage et al., 2013), which consequently have an effect on the Si^* . Even though the salinity minimum indicates mixing with water masses from the south, the SAMW is not clearly traceable any longer at a latitude of 14°S by its Si^* characteristics, which is most likely caused by admixture with other NO_3^- depleted water masses from the shelf to the study area and additionally by dissolution processes of bSiO_2 within the respective waters. St. 101 and St. 134 show low Si^* values ($-10 \mu\text{mol/kg}$) in 50 to 200 m depth with $\delta^{30}\text{Si}(\text{OH})_4$ values ranging from $+1.5\text{‰}$ to $+1.9\text{‰}$. These waters depth are influenced by current bands flowing eastward, like the SECC and SSCC, a oxygenated water mass from the Central Pacific (Fig. 5b). In summary we can say that we can identify several current bands and water masses with different origin, but they are not clearly distinguishable by distinct Si isotope signatures.

Additionally $\delta^{30}\text{Si}(\text{OH})_4$ could be influenced by hypoxic waters, which may have a significant effect on bSiO_2 dissolution processes given that enhanced bacterial activity (Diaz and Rosenberg, 2008) can lead to higher dissolution rates through the decay of the protecting organic layer (Bidle and Azam, 1999; Bidle et al., 2002; Demarest et al., 2011). Therefore, $\delta^{30}\text{Si}(\text{OH})_4$ signatures in waters with oxygen concentrations below $10 \mu\text{mol/kg}$ were compared with oxygen concentrations at different density surfaces (Fig. 6). The main extent of the OMZ in the study area ranges between neutral densities 26.25 to 27 kg/m^3 . Those waters show a large range in $\delta^{30}\text{Si}(\text{OH})_4$ signatures between $+1.1\text{‰}$ and $+1.9$ at similar density surfaces whereas $\text{Si}(\text{OH})_4$ concentrations remain rather constant between 22 and $40 \mu\text{mol/kg}$ (Fig. 6). If we look at similar density surfaces $\delta^{30}\text{Si}(\text{OH})_4$ show a large range, whereas $\text{Si}(\text{OH})_4$ is nearly constant. Different $\delta^{30}\text{Si}(\text{OH})_4$ in the OMZ corresponding to similar $\text{Si}(\text{OH})_4$ concentrations most likely reflect mixing of waters with different Si isotope signatures, even though the current band in these depth, as the SSCC and the EUC are not clearly distinguishable by different Si isotope signatures. A comparison with data adapted from Beucher et al. (2008), Supplementary Fig. A, from 110°W at similar neutral densities ($26.25 \text{ kg/m}^3 < \gamma^n < 27 \text{ kg/m}^3$) show that with higher oxygen concentrations further offshore $\delta^{30}\text{Si}(\text{OH})_4$ range only between $+1.5\text{‰}$ and $+1.7\text{‰}$ and $\text{Si}(\text{OH})_4$ concentrations vary from 15 to $35 \mu\text{mol/kg}$. Even though these $\delta^{30}\text{Si}(\text{OH})_4$ are less variable and $\text{Si}(\text{OH})_4$ concentrations are slightly lower the currently available data set cannot provide a clear answer to what extent the low oxygen concentrations within the OMZ have an influence on the Si isotope distribution. For a better understanding and distinction of the factors influencing the $\delta^{30}\text{Si}(\text{OH})_4$ distribution in these waters a detailed data set of the concentrations, as well the isotopic composition of particulate bSiO_2 and the diatom species assemblages of the same samples would be necessary.

Intermediate waters ($26.8 \text{ kg/m}^3 < \gamma^n < 27.4 \text{ kg/m}^3$, Fig. 2) in the study area show $\delta^{30}\text{Si}(\text{OH})_4$ values ranging from $+1.0\text{‰}$ to $+1.8\text{‰}$, with the lowest Si isotope compositions corresponding to the highest $\text{Si}(\text{OH})_4$ concentrations (Figs. 3 and 7). Fig. 7 shows a compilation with intermediate water samples from the Equatorial Pacific at 110°W (Beucher et al., 2008) and from the Southern and Equatorial Pacific (62°S to 12°S) along 103°W (De Souza et al., 2012b). While the highest $\delta^{30}\text{Si}(\text{OH})_4$ values of De Souza et al. (2012b) represent the SAMW/AAIW at their origin, $\delta^{30}\text{Si}(\text{OH})_4$ signatures decrease and $\text{Si}(\text{OH})_4$ concentrations increase while the water masses are subducted and flow towards the equator. In general, the main intermediate waters influencing the EEP are NPIW, AAIW, and EqPIW (Fig. 2) (e.g. Bostock et al., 2010), whereby EqPIW is the dominant water mass in the study area. AAIW, similar to SAMW is primarily formed in the southeast Pacific off the coast of southern Chile where it is subducted and flows northwards up to a latitude of approximately 20°S to 14°S (Wijffels, 1993; Talley, 1999; Kawabe and Fujio, 2010), whereas the NPIW is formed in the northwestern subtropical gyre along the Kuroshio and Oyashio Front (Talley, 1999) and is generally characterized by lower oxygen concentrations (150 mmol/kg) than its southern hemisphere counterpart, the AAIW ($200\text{--}300 \text{ mmol/kg}$, Table 1; Bostock et al., 2010). NPIW can be traced only to approximately 20°N and does not influence the study area directly (Fiedler and Talley, 2006). A study by Bostock et al. (2010) suggested that EqPIW, which extends approximately between 20°S and 20°N is not directly a mixture of AAIW and NPIW. This is supported for example by radiocarbon data that indicate an influence by lateral advection of an older deeper water mass, which could explain the lighter $\delta^{30}\text{Si}(\text{OH})_4$ signatures in intermediate waters of our study area.

In summary, the study area is characterized by a complex hydrographical system which is influenced by zonal current bands from the Central Pacific, as well as water masses, which are transported offshore from the shelf in addition to water masses from the south. These waters are not clearly distinguishable by distinct Si isotope signatures. In general the $\delta^{30}\text{Si}(\text{OH})_4$ rather reflects the Si^* properties of the water where more negative Si^* are associated to $\delta^{30}\text{Si}(\text{OH})_4$ values $> 1.5\text{‰}$. Oxygen concentrations does not seem to have an influence on $\delta^{30}\text{Si}(\text{OH})_4$. Consequently, the large range of Si isotope compositions in subsurface and intermediate waters is mainly the result of water mass mixing but may also be influenced by other processes, such dissolution.

4.3. Mixing of deep water masses

Deep water masses below 2000 m show an overall mean of $+1.2\text{‰} \pm 0.2\text{‰}$ ($1\sigma_{\text{sd}}$) which is within error in agreement with data from De Souza et al. (2012b), who investigated a transect from 62°S to 12°S in the eastern equatorial Pacific and other studies by Beucher et al. (2008, 2011) in the EEP (110°W , 140°W) showing a mean $\delta^{30}\text{Si}(\text{OH})_4$ of $+1.3\text{‰}$. Even though the overall mean values coincides well comparison with deep water masses from other areas of the Pacific Ocean reveal a large range of $\delta^{30}\text{Si}(\text{OH})_4$ between $+0.6\text{‰}$ and $+1.6\text{‰}$ (Fig. 8a), and are therefore clearly distinguishable considering the external error of the measurements (De La Rocha et al., 2000; Cardinal et al., 2005; Reynolds et al., 2006; Beucher et al., 2008, 2011; De Souza et al., 2012b; Cao et al., 2012). Fig. 8 shows a compilation of Pacific deep water (below 2000 m). Studies from the Central Pacific and the EEP (Beucher et al. 2008, 2011; De Souza et al., 2012b; this study) show an overall mean $\delta^{30}\text{Si}(\text{OH})_4$ of $+1.3 \pm 0.1\text{‰}$, which can not be distinguished by deep waters in the Southern Ocean near Australia (Cardinal et al., 2005), even though they show the lowest silicic acid concentrations. In contrast, waters from the deep North Pacific (Reynolds et al., 2006; De La Rocha

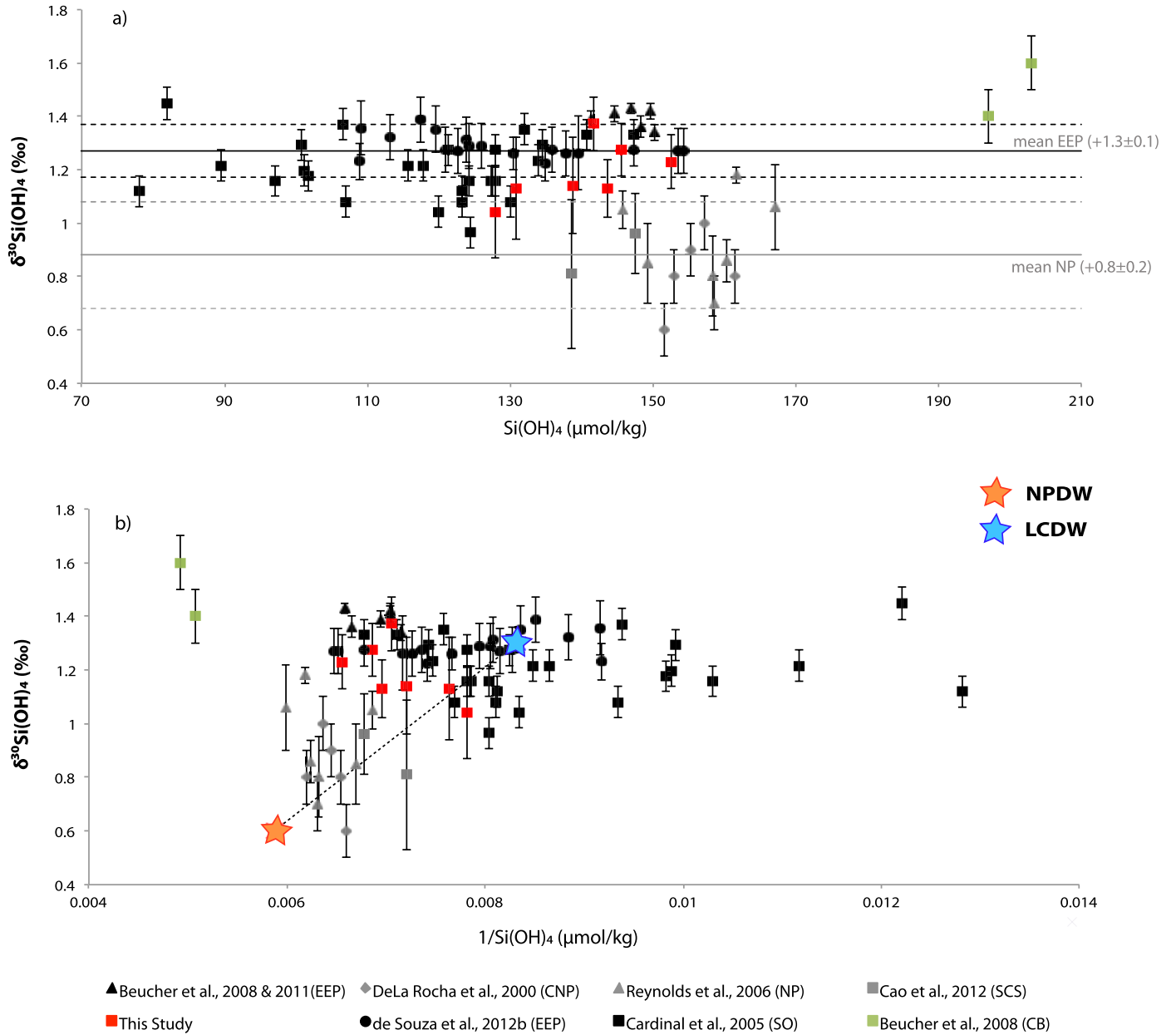


Fig. 8. (a) $\delta^{30}\text{Si}(\text{OH})_4$ versus silicic acid concentration (μmol/kg) for deep water samples collected below 2000 m water depth in the Pacific Ocean. (b) $\delta^{30}\text{Si}(\text{OH})_4$ versus $1/\text{Si}(\text{OH})_4$ (μmol/kg) with possible deep water end members in the study area. The data for NPDW is adapted from Reynolds et al. (2006) and De Souza et al. (2012b) for LCDW. The dashed line indicate a possible mixing line between NPDW and LCDW. Samples from the Eastern and Central Pacific are marked in black and red (black triangles, Beucher et al., 2008, 2011; black circles, De Souza et al., 2012b, red squares, this study), samples from the North Pacific and the South China Sea are marked in grey (grey triangle, Reynolds et al., 2006; grey square, Cao et al., 2012) and samples from the Southern Ocean near the Australian continent are shown in black (Cardinal et al., 2005). Deep water samples from the Cascadian Basin (Beucher et al., 2008) are marked in mint green. (For interpretation of the references to color in this figure legend, the reader is referred to the web version of this article.)

et al., 2000) and the South China Sea (Cao et al., 2012) show lower $\delta^{30}\text{Si}(\text{OH})_4$ values (+0.6‰ to +1.0‰) with a mean of $+0.8 \pm 0.2$ ‰. If we compare the data from the deep Pacific with possible end members, such as NPDW and LCDW (Reynolds et al., 2006; De Souza et al., 2012b) not all samples fall on a mixing line between these two water masses. As there is no clear systematic trend of the $\delta^{30}\text{Si}(\text{OH})_4$ signatures with $\text{Si}(\text{OH})_4$ concentrations it suggest that the data cannot be explained by a simple two end member mixing (Fig. 8b). De Souza et al. (2012b) suggested that the heterogeneity of Pacific deep water $\delta^{30}\text{Si}(\text{OH})_4$ rather reflects analytical uncertainties of previous studies in the northern Pacific and that no systematic variability in the deep Pacific can be observed. In our opinion there is, however, no reason to neglect the data obtained in the North Pacific. The North Pacific

and the Southern Ocean are the predominant regions for bSiO₂ dissolution (Sarmiento et al., 2007). $\text{Si}(\text{OH})_4$ accumulation predominantly occurs in the deep North Pacific as a function of aging of the deep water masses along their flow northward (Broecker, 1991), as well as $\text{Si}(\text{OH})_4$ discharge from the Cascadian Basin (Johnson et al., 2006). Even though the lighter $\delta^{30}\text{Si}(\text{OH})_4$ isotope signals in the western North Pacific can be explained by aging of the deep water masses and therefore accumulating of $\text{Si}(\text{OH})_4$, an explanation for the high $\delta^{30}\text{Si}(\text{OH})_4$ values (+1.6‰) in the Cascadian basin corresponding to high $\text{Si}(\text{OH})_4$ concentrations (> 160 μmol/kg) is challenging. According to Johnson et al. (2006) the silicate discharge plume may originate from crustal fluid venting. How this could cause such high $\delta^{30}\text{Si}(\text{OH})_4$ values remains unclear so far. Fluid venting should, similar to hy-

drothermal fluids, which are with values around -0.2‰ to -0.4‰ close to igneous rocks (-0.3‰) (Douthitt, 1982; Ding et al., 1996; De La Rocha et al., 2000), result in lower Si isotope compositions. In contrast, high $\delta^{30}\text{Si}(\text{OH})_4$ values ($+1.3\text{‰}$) in the Southern Ocean (De Souza et al., 2012a) can rather be explained by an admixture with $\text{Si}(\text{OH})_4$ depleted waters from the Atlantic. In summary, the factors controlling the large range of Si isotope signatures of the deep Pacific Ocean ($\delta^{30}\text{Si}(\text{OH})_4 = +0.6\text{‰}$ to $+1.6\text{‰}$) are not fully understood, but most likely a combination of several processes is responsible, which needs further investigation.

5. Conclusions

The distribution of the dissolved Si isotope composition of $\text{Si}(\text{OH})_4$ as well as of the $\text{Si}(\text{OH})_4$ concentration were analyzed in the Eastern Equatorial Pacific along two meridional transects from the equator to 14°S located between 100 and 1000 km off the Ecuadorian and Peruvian coast. Surface waters in the study area, in particular in its southern region, are strongly depleted in $\text{Si}(\text{OH})_4$, which leads to highly fractionated Si isotope compositions reaching $\delta^{30}\text{Si}(\text{OH})_4$ signatures of up to $+4.4\text{‰}$. This is most likely a function of northward advection of highly Si-depleted surface water masses into the study area from the coastal upwelling areas off Chile and Peru, which have undergone extensive diatom primary productivity. Different subsurface and intermediate water masses cannot be clearly distinguished in their $\delta^{30}\text{Si}(\text{OH})_4$ signatures given that the Si isotope distribution is not only a function of the mixing of water masses with distinct isotopic signatures but is also dependent on different contributions from the dissolution of bSiO_2 . The $\delta^{30}\text{Si}(\text{OH})_4$ signatures in subsurface intermediate water masses, in particular within the OMZ (50 m to 500 m) range from $+1.0\text{‰}$ to $+1.9\text{‰}$ and already reveal relatively light $\delta^{30}\text{Si}(\text{OH})_4$ signatures at shallow depths. Besides water mass mixing this could be due to enhanced bacterial degradation and therefore enhanced dissolution processes of diatom frustules within the OMZ. To achieve better constraints on the importance of oxygen levels on bSiO_2 dissolution a dedicated study including combined dissolved and particulate Si isotope distributions is required.

A compilation of all currently available deep water $\delta^{30}\text{Si}(\text{OH})_4$ data from the Pacific Ocean shows a large range from $+0.6\text{‰}$ to $+1.6\text{‰}$. Although water masses from the Northern Pacific show lower $\delta^{30}\text{Si}(\text{OH})_4$ values compared to the Central and Southern Pacific Ocean, there is no clear systematic trend with $\text{Si}(\text{OH})_4$ concentrations or distinct water masses. Thus it is suggested that the distribution of $\delta^{30}\text{Si}(\text{OH})_4$ signatures in deep waters of the Pacific are mainly controlled by mixing of more than two end member water masses combined with different Si isotope signal

Acknowledgements

This work is a contribution of the Sonderforschungsbereich 754 “Climate–Biogeochemistry Interactions in the Tropical Ocean” (www.sfb754.de), which is funded by the Deutsche Forschungsgemeinschaft. Special thanks go to the crew of the R/V Meteor for their support during cruises M77/3 and M77/4. We thank Damian Cardinal and 3 anonymous reviewers for their constructive criticism that substantially improved our paper.

References

Abrantes, F., Lopes, C., Mix, A., Pisias, N., 2007. Diatoms in Southeast Pacific surface sediments reflect environmental properties. *Quat. Sci. Rev.* 26, 155–169.

Albarède, F., Telouk, P., Blichert-Toft, J., Boyet, M., Agranier, A., Nelson, B., 2004. Precise and accurate isotopic measurements using multiple-collector ICPMS1. *Geochim. Cosmochim. Acta* 68, 2725–2744.

Altabet, M., Ryabenko, E., Stramma, L., Wallace, D., Frank, M., Grasse, P., Lavik, G., 2012. An eddy-stimulated hotspot for fixed nitrogen-loss from the Peru oxygen minimum zone. *Biogeosciences* 9, 4897–4908.

Amakawa, H., Sasaki, K., Ebihara, M., 2009. Nd isotopic composition in the central North Pacific. *Geochim. Cosmochim. Acta* 73 (16), 4705–4719, <http://dx.doi.org/10.1016/j.gca.2009.05.058>.

Aoki, S., Hariyama, M., Mitsudera, H., Sasaki, H., Sasai, Y., 2007. Formation regions of subantarctic mode water detected by OFES and Argo profiling floats. *Geophys. Res. Lett.* 34 (1), 10606, <http://dx.doi.org/10.1029/2007GL029828>.

Ayon, P., Criales-Hernandez, M., Schwaborn, R., Hirche, H., 2008. Zooplankton research off Peru: A review. *Prog. Oceanogr.* 79, 238–255.

Beucher, C., Brzezinski, M.A., Jones, J., 2008. Sources and biological fractionation of silicon isotopes in the Eastern Equatorial Pacific. *Geochim. Cosmochim. Acta* 72, 3063–3073.

Beucher, C.P., Brzezinski, M.A., Jones, J., 2011. Mechanisms controlling silicon isotope distribution in the Eastern Equatorial Pacific. *Geochim. Cosmochim. Acta* 75, 4286–4294.

Bidle, K.D., Azam, F., 1999. Accelerated dissolution of diatom silica by marine bacterial assemblages. *Nature* 397, 508–512.

Bidle, K.D., Manganello, M., Azam, F., 2002. Regulation of oceanic silicon and carbon preservation by temperature control on bacteria. *Science* 298, 1980–1984.

Bostock, H.C., Opdyke, B.N., Williams, M.J.M., 2010. Characterising the intermediate depth waters of the Pacific Ocean using $\delta^{13}\text{C}$ and other geochemical tracers. *Deep-Sea Res., Part 1, Oceanogr. Res. Pap.* 57, 847–859.

Brink, K., Halpern, D., Huyer, A., Smith, R.L., 1983. The physical environment of the Peruvian upwelling system. *Prog. Oceanogr.* 12, 285–305.

Broecker, W.S., 1991. The great ocean conveyor. *Oceanography* 4 (4), 79–89.

Cao, Z., Frank, M., Dai, M., Grasse, P., Ehlert, C., 2012. Silicon isotope constraints on sources and utilization of silicic acid in the northern South China Sea. *Geochim. Cosmochim. Acta* 97, 88–104.

Cardinal, D., Allemen, L.Y., Dehairs, F., Savoye, N., Trull, T., Andre, L., 2005. Relevance of silicon isotopes to Si-nutrient utilization and Si-source assessment in Antarctic waters. *Glob. Biogeochem. Cycles* 19, GB2007, <http://dx.doi.org/10.1029/2004GB002364>.

Chaigneau, A., Eldin, G., Dewitte, B., 2009. Eddy activity in the four major upwelling systems from satellite altimetry (1992–2007). *Prog. Oceanogr.* 83, 117–123.

Codispoti, L.A., 2007. An oceanic fixed nitrogen sink exceeding 400 Tg Na^{-1} vs the concept of homeostasis in the fixed-nitrogen inventory. *Biogeosciences* 4, 233–253.

Czeschel, R., Stramma, L., Schwarzkopf, F.U., Giese, S.B., Funk, A., Karstensen, J., 2011. Mid-depth circulation of the eastern tropical South Pacific and its link to the oxygen minimum zone. *J. Geophys. Res.* 116, C01015, <http://dx.doi.org/10.1029/2010JC006565>.

Daneri, G., Dellarossa, V., Quinones, R., Jacob, B., Montero, P., Ulloa, O., 2000. Primary production and community respiration in the Humboldt Current System off Chile and associated oceanic areas. *Mar. Ecol. Prog. Ser.* 197, 41–49.

De La Rocha, C., Brzezinski, M.A., DeNiro, M., 1997. Fractionation of silicon isotopes by marine diatoms during biogenic silica formation. *Geochim. Cosmochim. Acta* 61 (23), 5051–5056.

De La Rocha, C.L., Brzezinski, M.A., DeNiro, M.J., Shemesh, A., 1998. Silicon-isotope composition of diatoms as an indicator of past oceanic change. *Nature* 395, 680–683.

De LaRocha, C., Brzezinski, M.A., DeNiro, M.J., 2000. A first look at the distribution of stable isotopes of silicon in natural waters. *Geochim. Cosmochim. Acta* 64, 2467–2477.

De Souza, G., Reynolds, B., Rickli, J., Frank, M., Saito, M., Gerringa, L.J.A., Bourdon, B., 2012a. Southern Ocean control of silicon stable isotope distribution in the deep Atlantic. *Glob. Biogeochem. Cycles* 26, GB2035, <http://dx.doi.org/10.1029/2011GB004141>.

De Souza, G., Reynolds, B.C., Johnson, G.C., Bullister, J.L., Bourdon, B., 2012b. Silicon stable isotope distribution traces Southern Ocean export of Si to the eastern South Pacific thermocline. *Biogeosciences* 9, 4199–4213.

Demarest, M.S., Brzezinski, M.A., Beucher, C.P., 2009. Fractionation of silicon isotopes during biogenic silica dissolution. *Geochim. Cosmochim. Acta* 73, 5572–5583.

Demarest, M.S., Brzezinski, M.A., Nelson, D.M., Krause, J.W., Jones, J.L., Beucher, C.P., 2011. Net biogenic silica production and nitrate regeneration determine the strength of the silica pump in the Eastern Equatorial Pacific. *Deep-Sea Res. Part II* 58, 462–476, <http://dx.doi.org/10.1016/j.dsr2.2010.08.007>.

Diaz, R.J.R., Rosenberg, R.R., 2008. Spreading dead zones and consequences for marine ecosystems. *Science* 321 (5891), 926–929.

Ding, T., Jiang, S., Wang, D., Li, Y., Li, J., Song, H., Liu, Z., Lao, X., 1996. Silicon Isotope Geochemistry. Geological Publishing House.

Douthitt, C.B., 1982. The geochemistry of the stable isotopes of silicon. *Geochim. Cosmochim. Acta* 46, 1449–1458.

Ehlert, C., Grasse, P., Frank, M., 2013. Changes in silicate utilisation and upwelling intensity off Peru since the Last Glacial Maximum – Insights from silicon and neodymium isotopes. *Quat. Sci. Rev.* 72, 18–35.

Ehlert, C., Grasse, P., Mollier-Vogel, E., Bösch, T., Franz, J., de Souza, G.F., Reynolds, B.C., Stramma, L., Frank, M., 2012. Factors controlling the silicon isotope distribution in waters and surface sediments of the Peruvian coastal upwelling. *Geochim. Cosmochim. Acta* 99, 128–145.

Fiedler, P., Talley, L., 2006. Hydrography of the eastern tropical Pacific: A review. *Prog. Oceanogr.* 69, 143–180.

- Franz, J., Krahmann, G., Lavik, G., Grasse, P., Dittmar, T., Riebesell, U., 2012. Dynamics and stoichiometry of nutrients and phytoplankton in waters influenced by the oxygen minimum zone in the eastern tropical Pacific. *Deep-Sea Res., Part 1, Oceanogr. Res. Pap.* 62 (C), 20–31.
- Fripiat, F., Cavagna, A.-J., Savoye, N., Dehairs, F., André, L., Cardinal, D., 2011. Isotopic constraints on the Si–biogeochemical cycle of the Antarctic Zone in the Kerguelen area (KEOPS). *Mar. Chem.* 123, 11–22.
- Ganachaud, A.S., Sen Gupta, A., Orr, J.C., Wijffels, S.E., Ridgway, K.R., Hemer, M.A., Maes, C., Steinberg, C.R., Tribollet, A.D., Qiu, B., Kruger, J.C., 2011. Observed and expected changes to the tropical Pacific Ocean. In: Bell, J., Johnson, J.E., Hobday, A.J. (Eds.), *Vulnerability of Tropical Pacific Fisheries and Aquaculture to Climate Change*. Secretariat of the Pacific Community, Noumea, pp. 115–202.
- Georg, R.B., Reynolds, B., Frank, M., Halliday, A., 2006. New sample preparation techniques for the determination of Si isotopic compositions using MC-ICPMS. *Chem. Geol.* 235, 95–104.
- Grasse, P., Stichel, T., Stumpf, R., Stramma, L., Frank, M., 2012. The distribution of neodymium isotopes and concentrations in the Eastern Equatorial Pacific Water mass advection versus particle exchange. *Earth Planet. Sci. Lett.* 353–354, 198–207.
- Grasshoff, K., Kremling, K., Erhardt, M., 1999. *Methods for Seawater Analysis*, Third Completely Revised and Extended Version. Wiley–VCH, New York. 600 pp.
- Hauss, H., Franz, J.M.S., Sommer, U., 2012. Changes in N:P stoichiometry influence taxonomic composition and nutritional quality of phytoplankton in the Peruvian upwelling. *J. Sea Res.* 73, 74–85.
- Johnson, G.C., Toole, J.M., 1993. Flow of deep and bottom waters in the Pacific at 10°N. *Deep-Sea Res. Part 1* 40 (2), 371–394.
- Johnson, H.P., Hautala, S.L., Björklund, T.A., Zarnetske, M.R., 2006. Quantifying the North Pacific silica plume. *Geochim. Geophys. Geosyst.* 7 (5), Q05011, <http://dx.doi.org/10.1029/2005GC001065>.
- Kalvelage, T., Lavik, G., Lam, P., Contreras, S., Arteaga, L., Löscher, C.R., et al., 2013. Nitrogen cycling driven by organic matter export in the South Pacific oxygen minimum zone. *Nat. Geosci.* 6 (3), 228–234, <http://dx.doi.org/10.1038/ngeo1739>.
- Karl, D., Tien, G., 1992. MAGIC: A sensitive and precise methods for measuring dissolved phosphorus in aquatic environments. *Limnol. Oceanogr.* 37 (1), 105–116.
- Karstensen, J., Ulloa, O., 2008. The Peru–Chile Current System. *Encyclopedia of Ocean Sciences*. 2nd edition, online.
- Kawabe, M., Fujio, S., 2010. Pacific Ocean circulation based on observation. *J. Oceanogr.* 66, 389–403.
- Kessler, W., 2006. The circulation of the eastern tropical Pacific: A review. *Prog. Oceanogr.* 69, 181–217.
- Lam, P., Lavik, G., Jensen, M.M., Vossenberg, J., Schmid, M., Woebken, D., et al., 2009. Revising the nitrogen cycle in the Peruvian oxygen minimum zone. *PNAS* 106.
- Lewin, J., 1961. The dissolution of silica from diatom walls. *Geochim. Cosmochim. Acta* 21, 182–198.
- Matsumoto, K., Tokos, K., Huston, A., Joy-Warren, H., 2013. MESMO 2: a mechanistic marine silica cycle and coupling to a simple terrestrial scheme. *Geosci. Model Dev.* 6 (2), 477–494.
- McCartney, M.S., 1977. Subantarctic mode water. In: Angel, M. (Ed.), *A Voyage of Discovery, George Deacon 70th Anniversary Volume*. In: *Deep-Sea Res. (Suppl.)*. Pergamon, Oxford, pp. 103–119.
- Milligan, A.J., Varela, D.E., Brzezinski, M.A., Morel, F.M.M., 2004. Dynamics of silicon metabolism and silicon isotopic discrimination in a marine diatom as a function of $p\text{CO}_2$. *Limnol. Oceanogr.* 49 (2), 322–329.
- Penven, P., Echevin, V., Pasapera, J., Colas, F., Tam, J., 2005. Average circulation, seasonal cycle, and mesoscale dynamics of the Peru Current System: A modeling approach. *J. Geophys. Res.* 110 (C10), <http://dx.doi.org/10.1029/2005JC002945>.
- Pichevin, L.E., Reynolds, B.C., Ganeshram, R.S., Cacho, I., Pena, L., Keefe, K., Ellam, R.M., 2009. Enhanced carbon pump inferred from relaxation of nutrient limitation in the glacial ocean. *Nature* 459, 1114–1117.
- Redfield, A.C., 1958. The biological control of chemical factors in the environment. *Am. Sci.* 64, 205–221.
- Reynolds, B.C., Aggarwal, J., André, L., Baxter, D., Beucher, C.P., Brzezinski, M.A., Engström, E., et al., 2007. An inter-laboratory comparison of Si isotope reference materials. *J. Anal. At. Spectrom.* 22, 561.
- Reynolds, B., Frank, M., Halliday, A., 2006. Silicon isotope fractionation during nutrient utilization in the North Pacific. *Earth Planet. Sci. Lett.* 244, 431–443.
- Reynolds, B.C., Frank, M., Halliday, A.N., 2008. Evidence for a major change in silicon cycling in the subarctic North Pacific at 2.73 Ma. *Paleoceanography* 23, PA4216, <http://dx.doi.org/10.1029/2007PA001563>.
- Salée, J.-B., Speer, K., Rintouls, S., Wijffels, S., 2010. Southern Ocean thermocline ventilation. *J. Phys. Oceanogr.* 40, 509–529.
- Sarmiento, J.L., Gruber, N., Brzezinski, M.A., Dunne, J.P., 2004. High-latitude controls of thermocline nutrients and low latitude biological productivity. *Nature* 427, 57–60.
- Sarmiento, J.L., Simeon, J., Gnanadesikan, A., Gruber, N., Key, R.M., Schlitzer, R., 2007. Deep ocean biogeochemistry of silicic acid and nitrate. *Glob. Biogeochem. Cycles* 21, GB1S90, <http://dx.doi.org/10.1029/2006GB002720>.
- Schneider, W., 2003. Characteristics and formation of Eastern South Pacific Intermediate Water. *Geophys. Res. Lett.* 30 (11), 13.
- Strub, P.T., Mesias, J.M., Montecino, V., Rutllant, J., 1998. Coastal ocean circulation off western South America. *The Sea* 11, 273–313.
- Sutton, J.N., Varela, D.E., Brzezinski, M.A., Beucher, C.P., 2013. Species-dependent silicon isotope fractionation by marine diatoms. *Geochim. Cosmochim. Acta* 104, 300–309.
- Sweeney, E.N., McGillicuddy, D.J., Buesseler, K.O., 2003. Biogeochemical impacts due to mesoscale eddy activity in the Sargasso Sea as measured at the Bermuda Atlantic Time-series Study (BATS). *Deep-Sea Res., Part 2, Top. Stud. Oceanogr.* 50, 3017–3039.
- Talley, L., 1999. Some aspects of ocean heat transport by shallow, intermediate and deep overturning circulation. In: Clark, P.U., Webb, R.S., Keigwin, L.D. (Eds.), *Mechanisms of Global Climate change at Millennial Time Scales*. In: *Geophys. Monogr.*, vol. 112. American Geophysical Union, pp. 1–22.
- Toggweiler, J.R., Dixon, K., Broecker, W.S., 1991. The Peru upwelling and the ventilation of the South Pacific Thermocline. *J. Geophys. Res.* 96 (C11), 467–497.
- Tréguer, P., Nelson, D.M., van Bennekom, A.J., DeMaster, D.J., Leynard, A., Quéguiner, B., 1995. The silica balance in the world Ocean: a reestimate. *Science* 268, 375–379.
- Tschiya, M., Talley, L.D., 1998. A Pacific hydrographic section at 88°W: Water-property distribution. *J. Geophys. Res.* 103 (C6), 899–918.
- Wijffels, S.E. 1993. Exchanges between hemispheres and gyres: a direct approach to the mean circulation of the equatorial Pacific. Unpublished PhD thesis, MA Inst. Technol./Woods Hole Oceanogr. Inst. Joint Program Woods. Hole, MA.
- Wijffels, S., Toole, J., Bryden, H., Fine, R., Jenkins, W., Bullister, J., 1996. The water masses and circulation at 10°N in the Pacific. *Deep-Sea Res., Part 1, Oceanogr. Res. Pap.* 43 (4), 501–544.
- Winkler, L.W., 1888. Die Bestimmung des im Wasser gelösten Sauerstoffs. *Ber. Dtsch. Chem. Ges.* 21, 2843–2855.
- Wismeyer, A.G., 2003. Control mechanisms for the oceanic distribution of silicon isotopes. *Glob. Biogeochem. Cycles* 17 (3), 1083, <http://dx.doi.org/10.1029/2002GB002022>.